Hindawi Publishing Corporation
International Journal of Photoenergy
Volume 2012, Article ID 823498, 6 pages
doi:10.1155/2012/823498

Research Article

Effect of Fe Concentration on Fe-Doped Anatase TiO_2 from GGA + U Calculations

Hsuan-Chung Wu,[1,2] Sheng-Hong Li,[1] and Syuan-Wei Lin[1]

[1] *Department of Materials Engineering, Ming Chi University of Technology, 84 Gungjuan Road, Taishan, New Taipei 24301, Taiwan*
[2] *Center for Thin Film Technologies and Applications, Ming Chi University of Technology, New Taipei 24301, Taiwan*

Correspondence should be addressed to Hsuan-Chung Wu, hcwu@mail.mcut.edu.tw

Received 28 February 2012; Revised 23 May 2012; Accepted 29 May 2012

Academic Editor: Jincai Zhao

To comprehend the photocatalytic mechanisms of anatase $Ti_{1-x}Fe_xO_2$ with various concentrations of Fe, this study performed first principles calculations based on density functional theory with Hubbard U on-site correction to evaluate the crystal structure, impurity formation energy, and electronic structure. We adopted the effective Hubbard U values of 8.47 eV for Ti 3d and 6.4 eV for Fe 3d. The calculations show that higher concentrations of Fe are easily formed in anatase TiO_2 due to a reduction in the formation energy. The band gap of Fe-doped TiO_2 decreases Fe doping level increases as a result of the overlap among the Fe 3d, Ti 3d, and O 2p states, which enhances photocatalytic activity in the visible light region. Additionally, a broadening of the valence band and Fe impurity states within the band gap might also contribute to the photocatalytic activity.

1. Introduction

The increase in global pollution has led researchers to search for new techniques and materials to promote environmental protection. Since Fujishima and Honda's report in 1972 [1], the unique properties of TiO_2 have attracted considerable attention in the fields of air and water purification, hydrogen production, and dyesensitized solar cells. Anatase TiO_2 also has a wide band gap capable of only absorbing ultraviolet (UV) light ($\leq$387 nm). UV light accounts for a small fraction ($\sim$5%) of the available solar energy; therefore, the utilization of solar energy is low. To improve the photocatalysis of TiO_2, determining how to expand the optical absorption into the visible light region ($\sim$45%) has become a topic of considerable interest among researchers.

Considerable research has gone into modifying the band gap of TiO_2. One of the most effective methods involves doping TiO_2 crystals with impurities including transition metals, such as V [2], Mo [3], Fe [4–6], Co [7, 8], Pt [9], Au [10], and nonmetals such as N [11, 12], F [13], P [14], S [15]. Among these impurity elements, the radius of Fe^{3+} (0.64 Å) is similar to that of Ti^{4+} (0.68 Å) and is therefore easily incorporated into the TiO_2 crystal [16]. In addition, the Fe^{3+} dopant can serve as a charge trap, impeding the electron-hole combination rate and enhancing photocatalysis within a range suitable to the concentration of the dopant [17]. Fe is considered an appropriate candidate element and has been widely studied [18–25]. Zhang et al. [18] prepared Fe-doped mesoporous TiO_2 thin films and suggested that the doped Fe forms Fe^{3+} ions, which could play a role as e^- or h^+ traps, thereby reducing the e^-/h^+ pair recombination rate. Wang et al. [19] reported that the band gap of Fe-doped TiO_2 thin films decreased from 3.29 to 2.83 eV with an increase in the Fe^{3+} content from 0 to 25 wt%. The decrease in unit cell volume indicates that Fe^{3+} replaced Ti^{4+} in the lattice, forming a solid solution. Some experimental results [20, 21] have found that Fe doping in TiO_2 could narrow the band gap of TiO_2, thereby increasing the efficiency of the photocatalysis in the visible range. Yalçin et al. [22] performed calculations based on density function theory (DFT) to characterize the influence of Fe^{3+} doping on the electronic and structural properties of TiO_2. The results indicate that the visible light activity in Fe^{3+}-doped TiO_2 is due to the introduction of additional electronic states within the band gap.

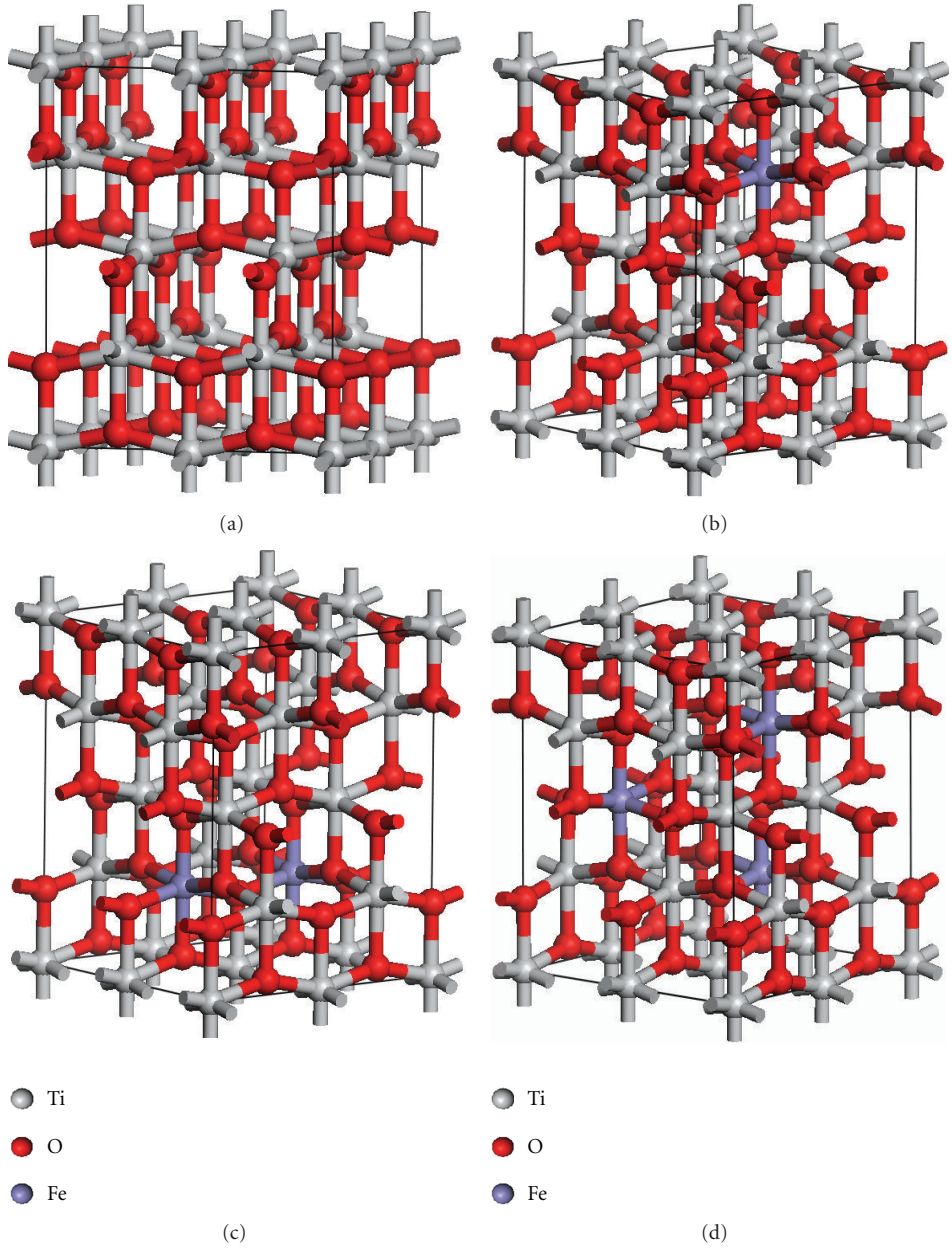

Figure 1: $2 \times 2 \times 1$ anatase TiO_2 supercell models with various concentrations of Fe: (a) pure TiO_2, (b) 2.08 at.%, (c) 4.17 at.%, (d) 6.25 at.%.

Recently, first-principles calculations were conducted for Fe-doped TiO_2, but these have been restricted to a single concentration of Fe [23–25]. To the best of our knowledge, few of these studies have focused on the photocatalytic mechanisms of Fe-doped anatase TiO_2 with different Fe concentrations. Additionally, most theoretical calculations have greatly underestimated the band gap of TiO_2 due to the adoption of the conventional DFT method, which is known to include an insufficient description of the on-site Coulomb interaction between electrons occupying the Ti 3d orbitals. This study performed first-principles calculations using the generalized gradient approximation + Hubbard U (GGA + U) approach to investigate the crystal structure, formation energy, and electronic structure of anatase $Ti_{1-x}Fe_xO_2$. Various concentrations of Fe, $x = 0.0625, 0.125$, and 0.1875 (2.08, 4.17, and 6.25 at.%), were analyzed.

2. Calculation Models and Methods

Anatase TiO_2 has a tetragonal structure with lattice parameters $a = b = 3.776$ Å, $c = 9.486$ Å. To calculate various concentrations of Fe, a $2 \times 2 \times 1$ supercell was constructed with 16 Ti and 32 O atoms, as shown in Figure 1(a). The calculations for the doping system were conducted for the $2 \times 2 \times 1$ supercell containing one, two, and three Fe atoms in the substitutional sites of the Ti atoms, as shown in Figures 1(b)–1(d), which correspond to the Fe concentrations of 2.08, 4.17, and 6.25 at.%, respectively.

First-principles calculations were performed using the CASTEP module [26] in Materials Studio 5.0 developed by Accelrys Software Inc. Electron-ion interactions were modeled using ultrasoft pseudopotentials in the Vanderbilt form [27]. The valence configurations of the atoms were $3s^2 3p^6 3d^2 4s^2$ for Ti, $2s^2 2p^4$ for O, and $3d^6 4s^2$ for Fe. The wave functions of the valence electrons were expanded through a plane wave basis-set and the cutoff energy was selected as 400 eV. The Monkhorst-Pack scheme [28] K-points grid sampling was set at $4 \times 4 \times 3$ (less than 0.04 $Å^{-1}$) in the supercells. The convergence threshold for self-consistent iterations was set at 5×10^{-6} eV. The lattice parameters and atomic positions for each supercell system were first optimized using the generalized gradient approximation (GGA) together with the method introduced by Wu and Cohen [29]. The optimization parameters were set as follows: energy change = 9×10^{-5} eV/atom, maximum force = 0.09 eV/Å, maximum stress = 0.09 GPa, and maximum displacement tolerance = 0.009 Å. To describe the electronic structures more accurately, the GGA + U method was adopted with the strong on-site Coulomb repulsion among the localized Ti 3d electrons described according to the following formalism [30, 31]:

$$E_{\mathrm{GGA}+U} = E_{\mathrm{GGA}} + \frac{U-J}{2}\sum_{\sigma}\mathrm{Tr}[\rho^{\sigma} - \rho^{\sigma}\rho^{\sigma}], \quad (1)$$

where ρ^{σ} denotes the spin (σ) polarized on-site density matrix. The spherically averaged Hubbard parameter U describes the increase in energy caused by the placement of an additional electron at a particular site, and the parameter J (1 eV) represents the screened exchange energy. The effective Hubbard parameter $U_{\mathrm{eff}} = U - J$, which accounts for the on-site Coulomb repulsion for each affected orbital, is the only external parameter required for this approach.

3. Results and Discussion

3.1. Structural Optimization. Table 1 summarizes the optimized lattice parameters, average bond lengths, and differences in volume, obtained from structure optimization. The optimized lattice parameters, $a = b = 3.778$ Å, and $c = 9.549$ Å, for pure anatase TiO_2 are in good agreement with the experimental values of $a = b = 3.782$ Å and $c = 9.502$ Å [32], indicating that our calculations are reliable. In anatase TiO_2, each Ti atom is bonded to its four nearest and two second nearest oxygen neighbors. Average bond lengths are represented as Ti–O^{1st} and Ti–O^{2nd}. With the same concentration of Fe, all of the Fe–O bond lengths are shorter than those of Ti–O. Therefore, the volume decreases with an increase in Fe concentration, which is consistent with the experimental results [33]. This indicates that Fe doping causes a contraction in the overall volume, which may be the result of the difference in the radii of the ions: 64 pm for Fe^{3+} and 68 pm for Ti^{4+}.

3.2. Hubbard U Parameter. The GGA + U approach uses an intra-atomic electron-electron interaction for on-site correction to describe systems with localized d and f electrons, capable of producing a more optimal band gap. Determining an appropriate Hubbard U_{eff} parameter is necessary in GGA + U calculations to correctly interpret the intra-atomic electron correlation. As shown in Figure 2, for anatase TiO_2, the band gap widens with an increase in the effective Hubbard U_{eff} of Ti 3d. The band gap was widened by increasing U_{eff} from 2 to 8 eV. Here, the on-site Coulomb interaction was $U_{\mathrm{eff}} = 8.47$ eV for Ti 3d using the GGA + U approach and the calculated band gap of pure anatase is 3.21 eV, which is close to the experimental value of 3.2 eV. Using the same method, the $U_{\mathrm{eff}} = 6.4$ eV of Fe 3d was determined by fitting the band gap of Fe_2O_3 (2.2 eV).

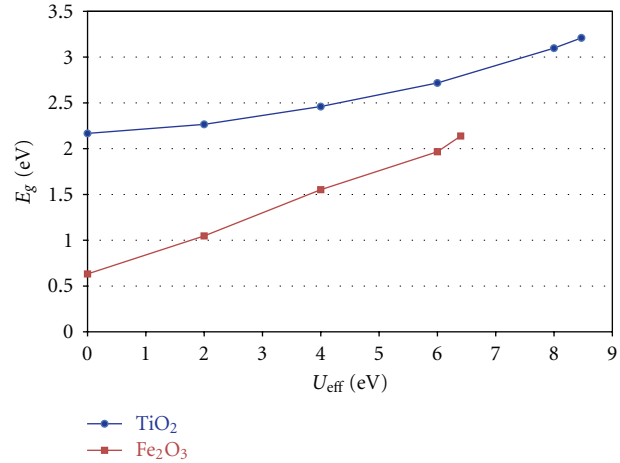

Figure 2: Relationship between the effective Hubbard parameter (U_{eff}) and the band gap (E_g) for anatase TiO_2 and Fe_2O_3.

3.3. Formation Energy. To examine the relative stability of TiO_2 doped with various concentrations of Fe, the defect formation energies were calculated according to the following formula:

$$E_f = E_{\mathrm{tot}}\ (\text{Fe-doped}) - E_{\mathrm{tot}}\ (\text{pure}) - n\mu_{\mathrm{Fe}} + n\mu_{\mathrm{Ti}}. \quad (2)$$

Here, E_{tot} (Fe-doped) and E_{tot} (pure) are the total energies of Fe-doped TiO_2 and pure TiO_2; n is the number of substitutional Fe atoms; μ_{Fe} and μ_{Ti} represent the chemical potentials of the Fe and Ti atoms, respectively. The formation energy depends on the growth conditions, which can be Ti-rich or O-rich. For TiO_2, μ_{Ti} and μ_{O} satisfy the relationship $\mu_{\mathrm{Ti}} + 2\mu_{\mathrm{O}} = \mu_{\mathrm{TiO_2}}$. Under the O-rich growth condition, μ_{O} is determined by the total energy of an O_2 molecule ($\mu_{\mathrm{O}} = \mu_{\mathrm{O_2}}/2$) and μ_{Ti} is determined by the formula $\mu_{\mathrm{Ti}} = \mu_{\mathrm{TiO_2}} - 2\mu_{\mathrm{O}}$. Under the Ti-rich growth condition, μ_{Ti} is the energy of one Ti atom in bulk Ti and μ_{O} is determined by $\mu_{\mathrm{O}} = (\mu_{\mathrm{TiO_2}} - \mu_{\mathrm{Ti}})/2$. The values of μ_{Ti} are -1601.80 and -1592.61 eV under the O-rich and Ti-rich, respectively. μ_{Fe} is the energy of one Fe atom in bulk Fe, and the calculated value is -856.33 eV. Table 2 summarizes the calculated formation energies for TiO_2 doped with various concentrations of Fe. It should be noted that the smaller the E_f value is, the easier it is to incorporate impurities into the TiO_2 supercell. The formation energy of Fe-doped TiO_2 is reduced to a greater degree under O-rich conditions than under

Table 1: Optimized lattice parameters, average bond lengths, and volume difference (ΔV) of TiO_2 doped with various concentrations of Fe.

Fe (at.%)	Lattice parameters (Å)			Bond lengths (Å)				ΔV (%)
	a	b	c	Ti–O^{1st}	Ti–O^{2nd}	Fe–O^{1st}	Fe–O^{2nd}	
0.00	3.778	3.778	9.549	1.931	1.986			
2.08	3.771	3.771	9.489	1.930	1.976	1.877	1.885	−1.00
4.17	3.759	3.732	9.591	1.923	1.992	1.891	1.903	−1.28
6.25	3.761	3.761	9.376	1.929	1.974	1.882	1.876	−2.67

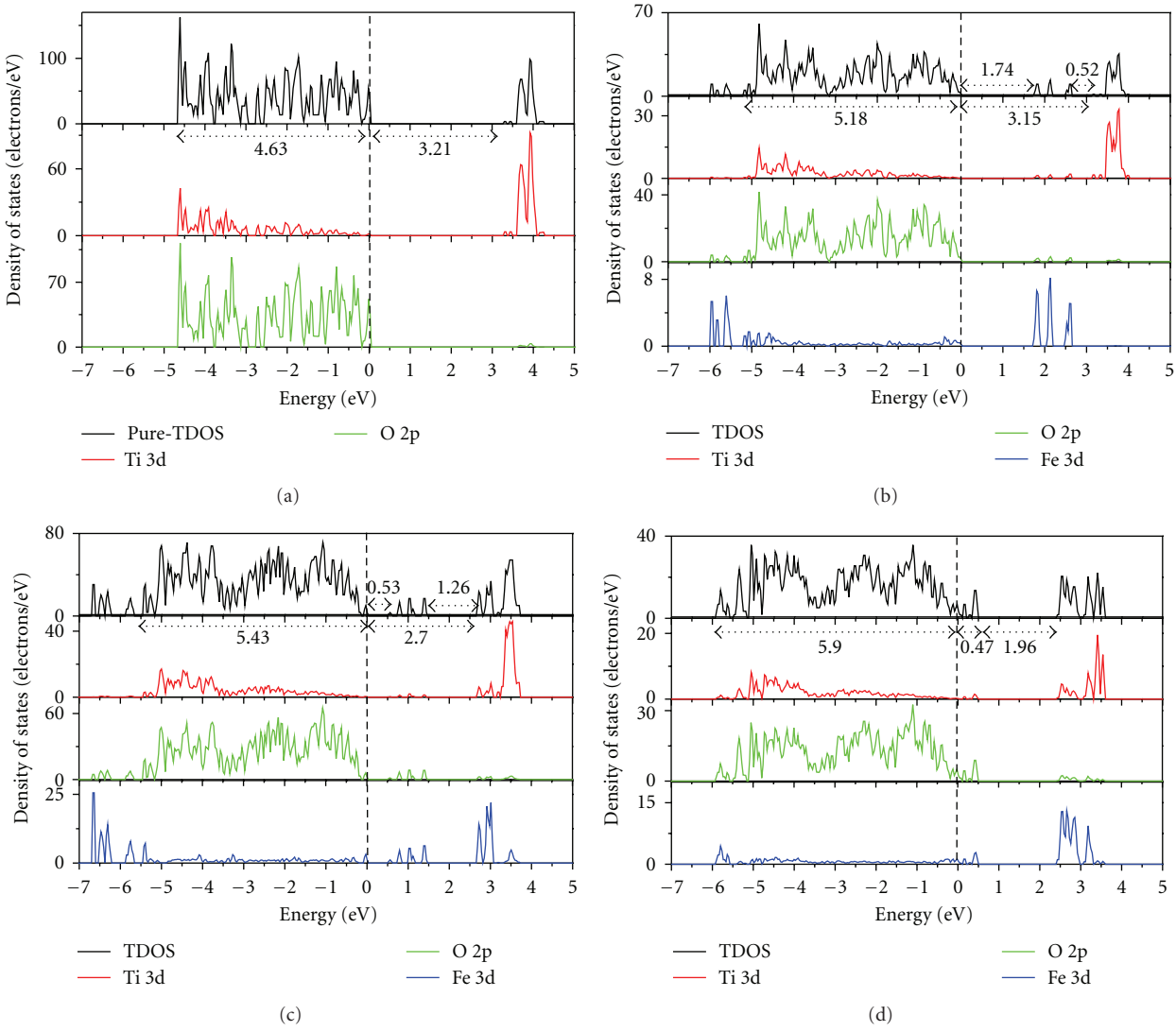

Figure 3: Density of states (DOS) of TiO_2 doped with Fe (a) 0 at.%, (b) 2.08 at.%, (c) 4.17 at.%, (d) 6.25 at.%. The vertical dotted line is the Fermi energy level.

the Ti-rich conditions, indicating that the incorporation of Fe into TiO_2 at the site of the Ti atom is favorable. In addition, the formation energies decrease with an increase in Fe concentration under O-rich conditions, suggesting that higher concentrations of Fe facilitate the synthesis of Fe-doped anatase TiO_2.

3.4. Electronic Structure. Figure 3 indicates the total density of states (TDOS), and the projected density of states (PDOS) to investigate the electronic properties of Fe-doped anatase TiO_2. The zero-point energy is taken as the Fermi level. The band gap (E_g) of pure anatase TiO_2 is 3.21 eV, as shown in Figure 3(a), and is consistent with the experimental value of 3.2 eV. In pure anatase TiO_2, the valence band (VB) mainly comprises O 2p states with a small number of Ti 3d states, while the conduction band (CB) comprises Ti 3d states with a small number of O 2p states. This indicates that there exists a little covalence bond character between Ti and O atoms. The valence band of TiO_2 has a large bandwidth (W_{VB}) of approximately 4.63 eV, showing

Table 2: Formation energy of $Ti_{1-x}Fe_xO_2$ for different Fe concentrations.

Fe (at.%)	Formation energy (eV)	
	O-rich	Ti-rich
2.08	−3.99	5.20
4.17	−10.01	8.36
6.25	−14.13	13.43

a strong delocalization among the O 2p electrons. At 2.08 at.% (Fe concentration) from Figure 3(b), we observe Fe 3d impurity states in the band gap ranging from 1.74 eV above the valence band maximum (VBM) to 0.52 eV below the conduction band minimum (CBM). The electrons in the VB can be excited to localized impurity states within the band gap and subsequently to the CB through the absorption of visible light. In addition, the substitutional Fe atom only transfers 3 electrons to the surrounding O atoms, which leads to unfilled O 2p orbitals and an electron remaining in the Fe^{3+} ion as shown in Figure 4. At 4.17 at.% (Figure 3(c)), the overlap of Fe 3d, Ti 3d, and O 2p bands near the CB results in a decrease in the CBM. Therefore, the band gap of Fe-doped TiO_2 at 4.17 at.% narrows to 2.70. From 4.17 at.% to 6.25 at.% (Figure 3(d)), the CBM continuously moves toward the Fermi level and hybridization among Fe 3d, Ti 3d, and O 2p near the Fermi energy level also occur, resulting in a reduced band gap. Figure 5 shows the relationships between E_g and W_{VB} and Fe concentration. E_g decreases with an increase in the Fe doping level, which is similar to other experimental results [18, 19]. It also reveals that the decrease in E_g from 2.08 at.% to 6.25 at.% is more obvious than that from 0 to 2.08 at.%. W_{VB} increases with an increase in Fe concentration due to the contribution from the lower Fe 3d band, which benefits the hole mobility in VB. As a result, the electron transition energy from the valence band to the conduction band decreases as a result of Fe-doping, which may induce a red shift at the edge of the optical absorption range. In addition, the valence band was found to broaden after Fe was incorporated into TiO_2 due to the contribution from the lower Fe 3d states. W_{VB} broadens with an increase in Fe concentration. The wider valence band results in an increase in the mobility of the photogenerated electron-hole pair. In this manner, both the narrowing of the band gap and the increased mobility of the photogenerated carriers can improve the photocatalytic activity under visible light.

4. Conclusions

This study used the GGA + U method to investigate the influence of doping concentration on the crystal structure, impurity formation energy, and electronic properties of Fe-doped anatase TiO_2. We adopted the effective Hubbard U values, 8.47 eV for Ti 3d and 6.4 eV for Fe 3d, to accurately determine the band gap in the experiments. The calculated results imply that higher concentrations of Fe facilitate the formation of anatase TiO_2. In addition, doping anatase TiO_2 with Fe can effectively narrow the band gap, thereby

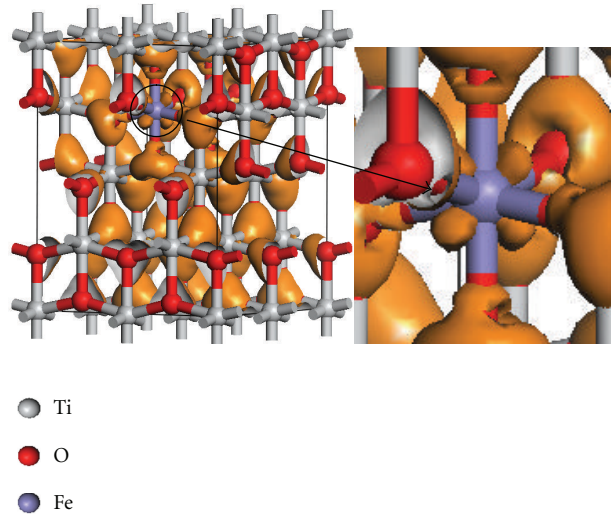

Figure 4: Charge distribution of Fe-doped TiO_2.

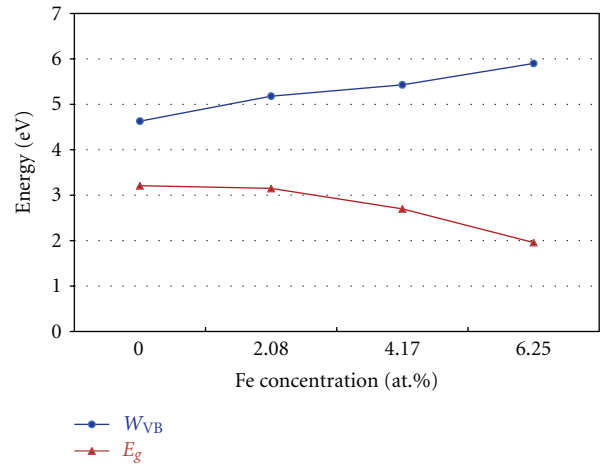

Figure 5: Relationship between band gap (E_g), valence band width (W_{VB}), and Fe concentration for Fe-doped TiO_2.

increasing photocatalytic activity in the visible light region and the trend of band gap decreases with an increase in Fe concentration. Both the broadening of the valence band and Fe impurity states within the band gap might also enhance photocatalytic activity.

Acknowledgments

This work was supported by the National Science Council in Taiwan (NSC 100-2221-E-131-017), for which the authors are grateful. They also acknowledge the National Center for High-performance Computing for computer time and the use of its facilities.

References

[1] A. Fujishima and K. Honda, "Electrochemical photolysis of water at a semiconductor electrode," *Nature*, vol. 238, no. 5358, pp. 37–38, 1972.

[2] I. Tsuyumoto and K. Nawa, "Thermochromism of vanadium-titanium oxide prepared from peroxovanadate and peroxotitanate," *Journal of Materials Science*, vol. 43, no. 3, pp. 985–988, 2008.

[3] Y. K. Du, Y. Q. Gan, P. Yang, F. Zhao, N. P. Hua, and L. Jiang, "Improvement in the heat-induced hydrophilicity of TiO_2 thin films by doping Mo(VI) ions," *Thin Solid Films*, vol. 491, no. 1-2, pp. 133–136, 2005.

[4] H. Yamashita, M. Harada, J. Misaka, M. Takeuchi, B. Neppolian, and M. Anpo, "Photocatalytic degradation of organic compounds diluted in water using visible light-responsive metal ion-implanted TiO_2 catalysts: Fe ion-implanted TiO_2," *Catalysis Today*, vol. 84, no. 3-4, pp. 191–196, 2003.

[5] S. Zhu, T. Shi, W. Liu et al., "Direct determination of local structure around Fe in anatase TiO_2," *Physica B*, vol. 396, no. 1-2, pp. 177–180, 2007.

[6] K. Naeem and F. Ouyang, "Preparation of Fe^{3+}-doped TiO_2 nanoparticles and its photocatalytic activity under UV light," *Physica B*, vol. 405, no. 1, pp. 221–226, 2010.

[7] M. Subramanian, S. Vijayalakshmi, S. Venkataraj, and R. Jayavel, "Effect of cobalt doping on the structural and optical properties of TiO_2 films prepared by sol-gel process," *Thin Solid Films*, vol. 516, no. 12, pp. 3776–3782, 2008.

[8] D. Sarkar, C. K. Ghosh, U. N. Maiti, and K. K. Chattopadhyay, "Effect of spin polarization on the optical properties of Co-doped TiO_2 thin films," *Physica B*, vol. 406, no. 8, pp. 1429–1435, 2011.

[9] X. Wenbin, D. Shurong, W. Demiao, and R. Gaochao, "Investigation of microstructure evolution in Pt-doped TiO_2 thin films deposited by rf magnetron sputtering," *Physica B*, vol. 403, no. 17, pp. 2698–2701, 2008.

[10] M. Zhou, J. Zhang, B. Cheng, and H. Yu, "Enhancement of visible-light photocatalytic activity of mesoporous Au-TiO_2 nanocomposites by surface plasmon resonance," *International Journal of Photoenergy*, vol. 2012, Article ID 532843, 10 pages, 2012.

[11] H. Fu, G. Shang, S. Yang, and T. Xu, "Mechanistic study of visible-light-induced photodegradation of 4-chlorophenol by $TiO_{2-x}N_x$ ($0.021 < x < 0.049$) with low nitrogen concentration," *International Journal of Photoenergy*, vol. 2012, Article ID 759306, 9 pages, 2012.

[12] J. Qian, G. Cui, M. Jing, Y. Wang, M. Zhang, and J. Yang, "Hydrothermal synthesis of nitrogen-doped titanium dioxide and evaluation of its visible light photocatalytic activity," *International Journal of Photoenergy*, vol. 2012, Article ID 198497, 6 pages, 2012.

[13] M. V. Dozzi, S. Livraghi, E. Giamello, and E. Selli, "Photocatalytic activity of S- and F-doped TiO_2 in formic acid mineralization," *Photochemical & Photobiological Sciences*, vol. 10, no. 3, pp. 343–349, 2011.

[14] Y. Lv, L. Yu, H. Huang, H. Liu, and Y. Feng, "Preparation, characterization of P-doped TiO_2 nanoparticles and their excellent photocatalystic properties under the solar light irradiation," *Journal of Alloys and Compounds*, vol. 488, no. 1, pp. 314–319, 2009.

[15] T. Umebayashi, T. Yamaki, H. Itoh, and K. Asai, "Band gap narrowing of titanium dioxide by sulfur doping," *Applied Physics Letters*, vol. 81, no. 3, pp. 454–456, 2002.

[16] M. Zhou, J. Yu, and B. Cheng, "Effects of Fe-doping on the photocatalytic activity of mesoporous TiO_2 powders prepared by an ultrasonic method," *Journal of Hazardous Materials*, vol. 137, no. 3, pp. 1838–1847, 2006.

[17] J. Zhang, Y. Wu, M. Xing, S. A. K. Leghari, and S. Sajjad, "Development of modified N doped TiO_2 photocatalyst with metals, nonmetals and metal oxides," *Energy and Environmental Science*, vol. 3, no. 6, pp. 715–726, 2010.

[18] Y. Zhang, Y. Shen, F. Gu, M. Wu, Y. Xie, and J. Zhang, "Influence of Fe ions in characteristics and optical properties of mesoporous titanium oxide thin films," *Applied Surface Science*, vol. 256, no. 1, pp. 85–89, 2009.

[19] M. C. Wang, H. J. Lin, and T. S. Yang, "Characteristics and optical properties of iron ion (Fe^{3+})-doped titanium oxide thin films prepared by a sol-gel spin coating," *Journal of Alloys and Compounds*, vol. 473, no. 1-2, pp. 394–400, 2009.

[20] W. Weng, M. Ma, P. Du et al., "Superhydrophilic Fe doped titanium dioxide thin films prepared by a spray pyrolysis deposition," *Surface and Coatings Technology*, vol. 198, no. 1–3, pp. 340–344, 2005.

[21] J. B. Naceur, R. Mechiakh, F. Bousbih, and R. Chtourou, "Influences of the iron ion (Fe^{3+})-doping on structural and optical properties of nanocrystalline TiO_2 thin films prepared by sol-gel spin coating," *Applied Surface Science*, vol. 257, no. 24, pp. 10699–10703, 2011.

[22] Y. Yalçin, M. Kiliç, and Z. Çinar, "Fe^{+3}-doped TiO_2: a combined experimental and computational approach to the evaluation of visible light activity," *Applied Catalysis B*, vol. 99, no. 3-4, pp. 469–477, 2010.

[23] X. Hou, M. Huang, X. Wu, and A. Liu, "First-principles calculations on implanted TiO_2 by 3d transition metal ions," *Science in China, Series G*, vol. 52, no. 6, pp. 838–842, 2009.

[24] Y. Su, Y. Xiao, Y. Li, Y. Du, and Y. Zhang, "Preparation, photocatalytic performance and electronic structures of visible-light-driven Fe-N-codoped TiO_2 nanoparticles," *Materials Chemistry and Physics*, vol. 126, no. 3, pp. 761–768, 2011.

[25] L. Jia, C. Wu, S. Han et al., "Theoretical study on the electronic and optical properties of (N, Fe)-codoped anatase TiO_2 photocatalyst," *Journal of Alloys and Compounds*, vol. 509, no. 20, pp. 6067–6071, 2011.

[26] M. D. Segall, P. J. D. Lindan, M. J. Probert et al., "First-principles simulation: ideas, illustrations and the CASTEP code," *Journal of Physics Condensed Matter*, vol. 14, no. 11, pp. 2717–2744, 2002.

[27] D. Vanderbilt, "Soft self-consistent pseudopotentials in a generalized eigenvalue formalism," *Physical Review B*, vol. 41, no. 11, pp. 7892–7895, 1990.

[28] H. J. Monkhorst and J. D. Pack, "Special points for Brillouin-zone integrations," *Physical Review B*, vol. 13, no. 12, pp. 5188–5192, 1976.

[29] Z. Wu and R. E. Cohen, "More accurate generalized gradient approximation for solids," *Physical Review B*, vol. 73, no. 23, Article ID 235116, 6 pages, 2006.

[30] S. L. Dudarev, G. A. Botton, S. Y. Savrasov, C. J. Humphreys, and A. P. Sutton, "Electron-energy-loss spectra and the structural stability of nickel oxide: an LSDA+U study," *Physical Review B*, vol. 57, no. 3, pp. 1505–1509, 1998.

[31] G. Shao, "Red shift in manganese- and iron-doped TiO_2: a DFT+U analysis," *Journal of Physical Chemistry C*, vol. 113, no. 16, pp. 6800–6808, 2009.

[32] J. K. Burdett, T. Hughbanks, G. J. Miller, J. W. Richardson, and J. V. Smith, "Structural-electronic relationships in inorganic solids: powder neutron diffraction studies of the rutile and anatase polymorphs of titanium dioxide at 15 and 295 K," *Journal of the American Chemical Society*, vol. 109, no. 12, pp. 3639–3646, 1987.

[33] C. Adán, A. Bahamonde, M. Fernández-García, and A. Martínez-Arias, "Structure and activity of nanosized iron-doped anatase TiO_2 catalysts for phenol photocatalytic degradation," *Applied Catalysis B*, vol. 72, no. 1-2, pp. 11–17, 2007.